Near-GeV-Energy Laser-Wakefield Acceleration of Self-Injected Electrons in a Centimeter-Scale Plasma Channel

F. S. Tsung,[1] Ritesh Narang,[2] W. B. Mori,[1,2] C. Joshi,[2] R. A. Fonseca,[3] and L. O. Silva[3]

[1]*Department of Physics and Astronomy , University of California, Los Angeles, Los Angeles, California 90095, USA*
[2]*Department of Electrical Engineering, University of California, Los Angeles, Los Angeles, California 90095, USA*
[3]*GoLP/Centro de Fisica dos Plasmas, Instituto Superior Tecnico, 1049-001 Lisboa, Portugal*

(Received 24 October 2003; published 27 October 2004)

The first three-dimensional, particle-in-cell (PIC) simulations of laser-wakefield acceleration of self-injected electrons in a 0.84 cm long plasma channel are reported. The frequency evolution of the initially 50 fs (FWHM) long laser pulse by photon interaction with the wake followed by plasma dispersion enhances the wake which eventually leads to self-injection of electrons from the channel wall. This first bunch of electrons remains spatially highly localized. Its phase space rotation due to slippage with respect to the wake leads to a monoenergetic bunch of electrons with a central energy of 0.26 GeV after 0.55 cm propagation. At later times, spatial bunching of the laser enhances the acceleration of a second bunch of electrons to energies up to 0.84 GeV before the laser pulse intensity is significantly reduced.

DOI: 10.1103/PhysRevLett.93.185002 PACS numbers: 52.38.Kd, 52.59.–f

One of the major goals of the ultrahigh-gradient, plasma-based acceleration schemes is to demonstrate a 1 GeV compact plasma accelerator driven by a tabletop terawatt (T^3) laser [1]. To reach 1 GeV energies, the laser must be kept focused without significant longitudinal and transverse breakup over many Rayleigh lengths [2]. In addition, it is desirable that the beam be mono-energetic. In this Letter we explore for the first time the laser-wakefield acceleration of self-injected electrons in centimeter-scale plasma channels using the 3D, particle-in-cell (PIC) code framework OSIRIS [4]. The 3D results differ from linear theory and 2D PIC simulations and shed light on what is likely to happen in near term experiments.

We assume the laser wavelength, $\lambda_0 = 2\pi/k_0 = 0.8\ \mu$m. We use a computational window of dimension $136\ \mu\text{m} \times 136\ \mu\text{m} \times 136\ \mu$m which moves at the speed of light, c. The number of gridpoints is $3712 \times 256 \times 256 = 2.4 \times 10^8$. The transverse plasma profile for both electrons and ions is a leaky channel [3] parametrized as $n(r) = n_0[1 + \Delta n/n_0(r^2/w_0^2)]$ for $r \equiv \sqrt{y^2 + z^2} < r_1$ and with n falling linearly from $n(r_1)$ to 0 for $r_1 < r < r_2$. The resolution in the transverse direction is $k_{p0}\Delta y = 0.17$, where $k_{p0} = \omega_{p0}/c$, $k_0/k_{p0} = 24.13$, and $\omega_{p0}^2 \equiv 4\pi e^2 n_0/m$. We use four electrons/cell (2×10^8 particles total) and a smooth neutralizing immobile ion background. A diffraction limited laser pulse is focused at the channel entrance with a spot size w_0.

The parameters for our 3D simulation were chosen using physics considerations, linear theory [2] as a guide, and numerous 2D PIC simulations. The laser pulse length τ_{FWHM} (FWHM of intensity) was 50 fs and power (13 TW) were chosen to be well within current laser technology. The focused spot size, 7.4 μm, was chosen so the focused intensity, $I = 1.5 \times 10^{19}$ W/cm^2, i.e., the normalized vector potential $a \equiv (eA)/(mc^2) = 3$, would lead to wakes approaching but below the so-called wave breaking limit [5]. The laser pulse is Gaussian in the transverse direction and has a symmetric fifth order polynomial temporal profile. The density, n_0, was chosen to provide the largest wake for the given pulse length and to provide a long enough dephasing length to obtain GeV electrons, Δn was chosen to guide the laser pulse with little spot size oscillations, and r_1 was chosen so that the simulation would provide insight into how an unmatched laser couples into a channel. These considerations for the 3D simulation lead to $n_0 = 3 \times 10^{18}$ cm^{-3}, $\Delta n = 6 \times 10^{18}$ cm^{-3}, $w_0 = 7.4\ \mu$m, $r_1 = 7\ \mu$m, and $r_2 = 17\ \mu$m. The value of Δn is 3 times larger than $\Delta n_c = 2 \times 10^{18}$ cm^{-3}, which is the theoretical value for guiding in the absence of nonlinearities.

The prediction for the key experimental observable is summarized in Fig. 1 where the maximum energy of any electron is plotted versus laser propagation distance for identical 2D and 3D simulations and the distribution function of the accelerated electrons [$f(E)$ vs E] is plotted at two propagation distances (0.5 and 0.9 cm) for the 3D case. In Fig. 1(a), it can be seen that when the laser initially enters the plasma, there are no self-injected electrons in either the 2D or 3D runs. However, after some distance (~0.25 cm in 3D), electrons become "self-injected" into the plasma wave. These electrons are rapidly accelerated to nearly 0.48 GeV in a distance of only 0.25 cm, with a peak gradient of 350 GeV/m. The normalized emittances of this bunch (particles between 200 to 400 MeV) $[\varepsilon_N]_i = \pi/c[\langle \Delta u_i^2 \rangle \langle \Delta x_i^2 \rangle - \langle \Delta x_i \Delta u_i \rangle^2]^{1/2}$ are 18.64 and 73.24 μm along the direction of the oscillating magnetic ($\hat{b}$) and electric fields ($\hat{e}$) of the laser, respectively. The maximum electron energy saturates and then decreases as these electrons diphase in the wave. A beam with similar energy was observed in simulations reported by others [6] for a much higher laser

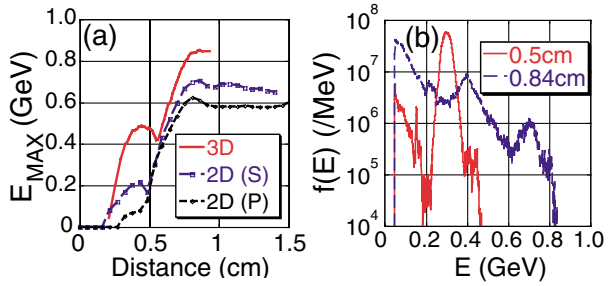

FIG. 1 (color). (a) Maximum electron energy, E_{MAX}, as a function of laser propagation distance in the plasma channel. (b) The accelerated electron distribution functions at two distances in the channel in 3D simulations ($E > 10$ MeV). The beam propagates in vacuum for 0.04 cm after exiting the plasma.

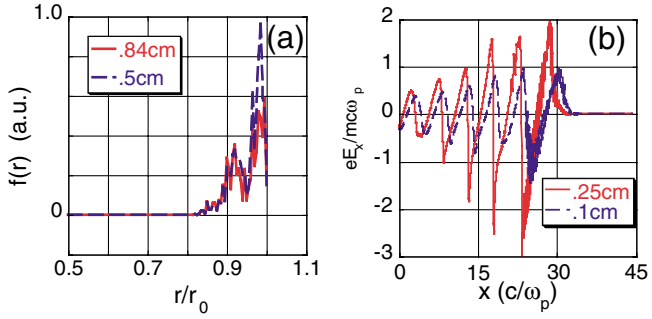

FIG. 2 (color). (a) The distribution of radial position at which the electrons shown in Fig. 1(b) originated. (b) The longitudinal component of the wakefield taken after the laser enters the channel (0.1 cm) and when electrons are self-injected (0.25 cm).

power in a uniform plasma. At a distance of 0.55 cm, a distinct second group of self-injected particles is observed. These electrons eventually reach an energy of 0.84 GeV. As shown in Fig. 1(b), the acceleration of the first group of self-injected electrons results in a beam with a 20% energy spread, whereas the second group has a continuous energy spread. The small energy spread of the former is produced as the particles rotate in (p_x, x) phase space as the higher p_x particles decelerate.

For both propagation distances used in Fig. 1(b), the number of self-injected electrons is large. Integrating the curves in Fig. 1(b) gives 0.52 nC for 0.5 cm and 0.66 nC for 0.84 cm. Figure 1(a) also shows that there are differences between 2D and 3D. The biggest difference is that the energy of the first group of self-injected electrons and their rate of acceleration is much lower in 2D [both with the laser polarized in (P) or out (S) of the simulation plane]. This is due to the differences in the wake structure in the blowout regime between 2D slab and 3D geometries. Furthermore, the maximum energy of the second bunch is more than 20% lower for the 2D cases.

The self-injected electrons all come from near the channel walls, which is clearly shown in Fig. 2(a) where we plot the distribution line of each high energy electrons (> 5 MeV) against their original radical positions shown in Fig. 1(b). Furthermore, as the laser enters the channel, the initial wake is less than unity in normalized $(mc\omega_{p0}/e)$ units. This is illustrated in Fig. 2(b) where lineouts of the wake are plotted for the two cases: before the laser is significantly modified by the plasma (blue) and where self-injection begins to occur (red). In these units, wave breaking (self-trapping) in 1D does not occur until the wave greatly exceeds 1. Therefore, it is not expected that self-injection would ever occur. However, as shown in Fig. 2(b), the wake amplitude and structure change dramatically as the laser's shape and amplitude evolve self-consistently in the channel, leading to self-injection from the channel wall.

In the absence of a definitive theory for how self-injection occurs in the blowout regime [7], we start from the constant of the motion for an individual electron which is not trapped [8], $\gamma_{\mathrm{eff}} - p_x - (1 + \psi) = 0$, where $\gamma_{\mathrm{eff}} = (1 + p_x^2 + p_y^2 + p_z^2 + |a|^2/2)^{1/2}$, the momenta are normalized to mc, and the potential $\psi \equiv e(\phi - A_x)/mc^2$ can be solved for via $-\nabla_\perp^2 \psi = \rho - j_x$, where $\nabla_\perp^2 = \partial_y^2 + \partial_z^2$ and ρ and j_x are normalized to en_0 and $en_0 c$, respectively. In the blowout regime, plasma electrons are completely evacuated radially out to a blowout radius r_b. The charge density ρ is therefore due to an ion column of radius r_b, and a narrow sheath of blowout electrons.

From the constant of motion γ_{eff}, the parallel velocity, v_x normalized to c can be written as

$$v_x = \frac{(1 + p_\perp^2 + |a|^2/2) - (1 + \psi)^2}{(1 + p_\perp^2 + |a|^2/2) + (1 + \psi)^2}, \qquad (1)$$

where $p_\perp^2 \equiv p_y^2 + p_z^2$. In order for a particle to be trapped, v_x must exceed the phase velocity of the wake, $v_{\phi w}$, in a region of focusing fields (note that the expression for γ_{eff} breaks down for v_x near the speed of light). This is different from that described in Ref. [9], which was based on a gradual deformation of the wake due to a transverse dependence on the wake's frequency.

Another requirement for self-injection is that the ponderomotive force causes electrons from near the radial axis to cross electrons that originate at the edge of the channel. Only then can electrons at the edge be attracted inwards and arrive on axis before the bulk of the electrons that constitute the sheath. In the simulations presented here, the value of r_1 is nearly w_0. The trajectory crossing requirement [10] could also be met in a uniform plasma or wide channel. If $r_1 \gg w_0$, then the blowout radius needs to approach or exceeds w_0, not r_1, and the self-injected electrons would originate there. However, trajectory crossing can more easily occur in a channel because the restoring force is larger for a given electron displacement for electrons in regions of higher ion density.

We can estimate the requirement for trajectory crossing by setting the blowout radius to $\sim w_0$. For a parabolic channel, the potential ψ on the axis is given by

$$\psi = \alpha k_{p0}^2 r_b^2 \left(1 + \beta \frac{\Delta n}{n_0} \frac{r_b^2}{w_0^2}\right) + \psi_s, \qquad (2)$$

where ψ_s represents a negative contribution from the electron sheath and r_b is a function of $ct - z \equiv \zeta$. The coefficients α and β are 1/4 and 1/4 in 3D and 1/2 and 1/6 in 2D slab geometry. By equating $(1 + \psi) = (1 + |a|^2/2)^{1/2}$ on the axis for ψ given in Eq. (2), we estimate that for the blowout radius r_b to approach r_1 the normalized vector potential, a, must exceed 4.30 in 3D and 5.36 in 2D. This is one reason why the wake amplitude and the self-injection does not occur until the lasers peak vector potential evolves from an initial value of 3 to a value of 5.

For large values of r_b, where ψ greatly exceeds unity, the electrons will return to the axis with a large $p_\perp$ and for the simulation parameters used here, the ponderomotive potential vanishes at this position. Furthermore, as the electrons converge to the axis, the ion column radius decreases so that ψ is dominated by the negative contribution from the electron sheath, ψ_s (in the simulations $\psi_s = 0.5$ at the convergence position). The large values of $p_\perp$ and ψ being negative both contribute to make v_x approach unity leading to self-injection.

In Figs. 3(a) and 3(b) lineouts of the laser's vector potential and in Fig. 3(c) the lineout of the electric field are shown at various propagation distances in units of the initial peak fields. Each plot also shows the initial laser profile. At the distance when the first stage of self-injection occurs, 0.25 cm, the vector potential [Fig. 3(a)] of the laser shows the expected self-phase modulation due to the wake, with photon frequency being down-shifted at the front and up-shifted at the back. Photon acceleration/deceleration (PA/PD) [11] results when there is a gradient in the index of refraction, causing phase fronts to catch up/fall behind each other. In the blowout regime, PA/PD is very localized because the gradients in the index of refraction occur either at the front or the back of the blowout region. At the front, the ponderomotive force snowplows the density, leading to rapid PD to substantially lower frequencies. The middle of the pulse propagates nearly at c in the vacuum region, while the back undergoes PA to higher frequencies by the density compression caused by the convergence of the blow-out electrons. This regime is very different from that recently studied by Gordon *et al.* [12], who studied the ultrashort pulse regime in which the entire pulse is photon decelerated.

As seen in Figs. 3(a) and 3(b), PD combined with group velocity dispersion modifies the vector potential and electric fields differently, i.e., $E_z = 1.4$ and $a > 2$ times their initial values. The value of a has increased more because PD acts like a ponderomotive force, or $|a|^2$ amplifier. Although the energy in the laser decreases due to pump depletion, the number of photons or, equivalently, the action, $|E|^2/\omega = \omega|a|^2$ is conserved locally [11]. Therefore, pump depletion (due to PD) leads to an increase in the ponderomotive force which increases the blowout radius and the wake's amplitude.

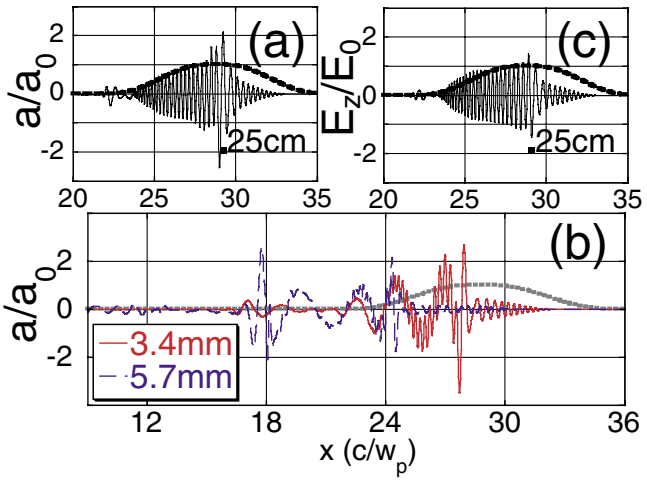

FIG. 3 (color). (a), (b) The vector potential and (c) the electric field both normalized to their initial values in the plasma channel. The dotted lines are the initial envelope of the laser. The horizontal scale is $x(c/\omega_p)$ in (a), (b), and (c).

At $x = 0.34$ cm (the red curve in Fig. 3(c)), one sees clearly the combined effect of self-phase modulation and group velocity dispersion. At this time, the laser pulse is not only broader, but the frequency content of the pulse has been rearranged by group velocity dispersion. Now the higher frequency components are at the front of the pulse while the lower frequency photons have slipped to the back. As the low frequency photons slip backward to the density compression at the back, they are eventually photon accelerated back to higher frequencies. This leads to the pulse appearing as two short pulses at the front and back of the blown-out region, as shown in the blue curve in Fig. 3(c).

In Fig. 4, a sequence of density contours are shown in two transverse planes, $n(x, y, z = 0)$ and $n(x, y = 0, z)$ for

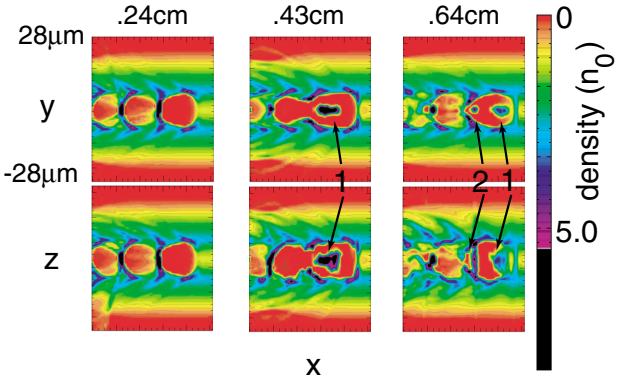

FIG. 4 (color). Electron density contour showing the wake structure at three different locations in the channel in (z vs x) and out (y vs x) of the plane of the electric field of the laser. 1 and 2 are the locations of the first and second self-injected electron bunch, respectively.

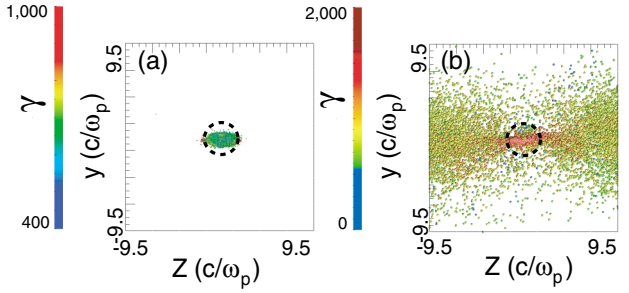

FIG. 5 (color). End on view of the transverse distribution of high energy particles at (a) $x = 0.5$ cm and (b) at $x = 0.84$ cm. The circle denotes the ring of peak density of the original plasma channel.

3 propagation distances. We only show the region surrounding the first two buckets. The plots at $x = 0.24$ cm show the density contours before self-injection. Here all electrons within the channel are blown out and the wake is reasonably symmetric. At $x = 0.43$ cm, the first self-injected bunch is clearly seen in both planes. It remains confined in the bucket by the focusing fields (radial electric field) of the ion channel. (Note that the self-fields of the beam nearly vanish to order γ^2.) By this time, the particles have significantly slipped forward with respect to the wake as the front of the laser continues to be pump depleted.

The amount of charge in this bunch is significant enough to modify the structure of the wake through beam loading. The modification of the wake is due to both the radial electric field (the magnetic field forces are smaller for the plasma particles since they are not moving forward at c of the trapped electrons as well as the locally enhanced ponderomotive force (vector potential) of the laser in the rear of the first bucket [see Fig. 3(c)] opposing the ion channel force in returning the blown-out electrons to the axis. Therefore, the expelled electrons no longer cross the axis, leaving an ion channel on axis up to the end of the second bucket. This also prevents further self-trapping and is what leads to a monoenergetic beam. At this point, the peak energy of the trapped electrons has saturated at $\sim$0.48 GeV as the highest energy electrons are now in the zero field region. As the laser continues to evolve, its group velocity continues to decrease which causes the bunch to phase slip more rapidly. Eventually, the electrons in the front of the bunch start to be decelerated causing the first bunch to rapidly rotate in phase space leading to a beam with a central energy of 0.26 GeV, but with the reduced energy spread as shown in Fig. 1(b).

As the laser propagates further, the first bunch continues to slip forward with respect to the laser, where it completely enters the decelerating phase of the wake and therefore loses energy. By $x = 0.43$ cm, it resides in an area of the first bucket for which its own radial electric field increases the blow-out radius which leads to a distinct second bunch of self-injected electrons in the first bucket. This is seen in the $x = 0.64$ cm plots of Fig. 4. This second bunch is accelerated by both the longitudinal electric field of the wake as well as the strong localized electric field of the laser. The laser is tightly focused in this region so it also has a strong axial component.

By $x = 0.69$ cm (not shown), the first bunch has completely been decelerated by the front of the wake; however, electrons in the second self-trapped bunch continue to increase in energy up to a maximum energy of 0.84 GeV (as shown in Fig. 1(a)]. At $x = 0.84$ cm, the laser is essentially depleted of its energy as is the wake and the acceleration process saturates.

Finally, as Fig. 5(a) shows, the first bunch remains confined within the plasma channel, whereas the second bunch, Fig. 5(b), spreads mainly transversely as these latter electrons oscillate in the laser electric field. This can also be seen in Fig. 4. However, the highest energy electrons (red dots) belonging to the second bunch still are predominantly confined within the channel. Although the total charge in the first and second bunch is comparable, the first bunch has both a much better transverse emittance and a narrower energy spread compared to the much higher energy second bunch.

This work is supported by DOE under Grants No. DE-FE02-01ER41179, No. DE-FG03-92-ER4727, No. DE-FG52-03NA00065, DE-FG02-3ER54721, and by FCT (Portugal). The simulations were performed on the IBM SP @ NERSC.

[1] C. Joshi and T. Katsouleas, Phys. Today **56**, 47 (2003).
[2] W. P. Leemans *et al.*, IEEE Trans. Plasma Sci. **24**, 331 (1996) and references therein; P. Sprangle *et al.*, Phys. Rev. E **63**056405 (2001).
[3] H. M. Milchberg *et al.*, Phys. Plasmas **3**, 2149 (1996).
[4] R. G. Hemker *et al.*, *Proceedings of the 1999 Particle Accelerator Conference*, edited by A. Luccio and W. MacKay (IEEE, Piscataway, NJ, 1999), Vol. 5, p. 3672; R. Fonseca *et al.*, *Lecture Notes in Computer Science* (Springer, Heidelberg, 2002), Vol. 2329, III-342.
[5] T. Katsouleas and W. B. Mori, Phys. Rev. Lett. **61**, 90 (1988).
[6] A. Pukhov and J. Meyer-Ter-Vehn, Appl. Phys. B **B74**, 355 (2002).
[7] J. B. Rosenzweig, B. Breizman, T. Katsouleas, and J. J. Su, Phys. Rev. A **44**, R6189 (1991).
[8] P. Mora and T. M. Antonsen, Phys. Plasmas **4**, 217 (1997).
[9] S. V. Bulanov *et al.*, Phys. Rev. Lett. **78**, 4205 (1997).
[10] J. M. Dawson, Phys. Rev. **113**, 383 (1959).
[11] W. B. Mori, IEEE J. Quantum Electron. **33**, 1942 (1997) and references therein; F. S. Tsung *et al.*, Proc. Natl. Acad. Sci. U.S.A. **99**, 29 (2002).
[12] D. F. Gordon *et al.*, Phys. Rev. Lett. **90**, 215001 (2003).